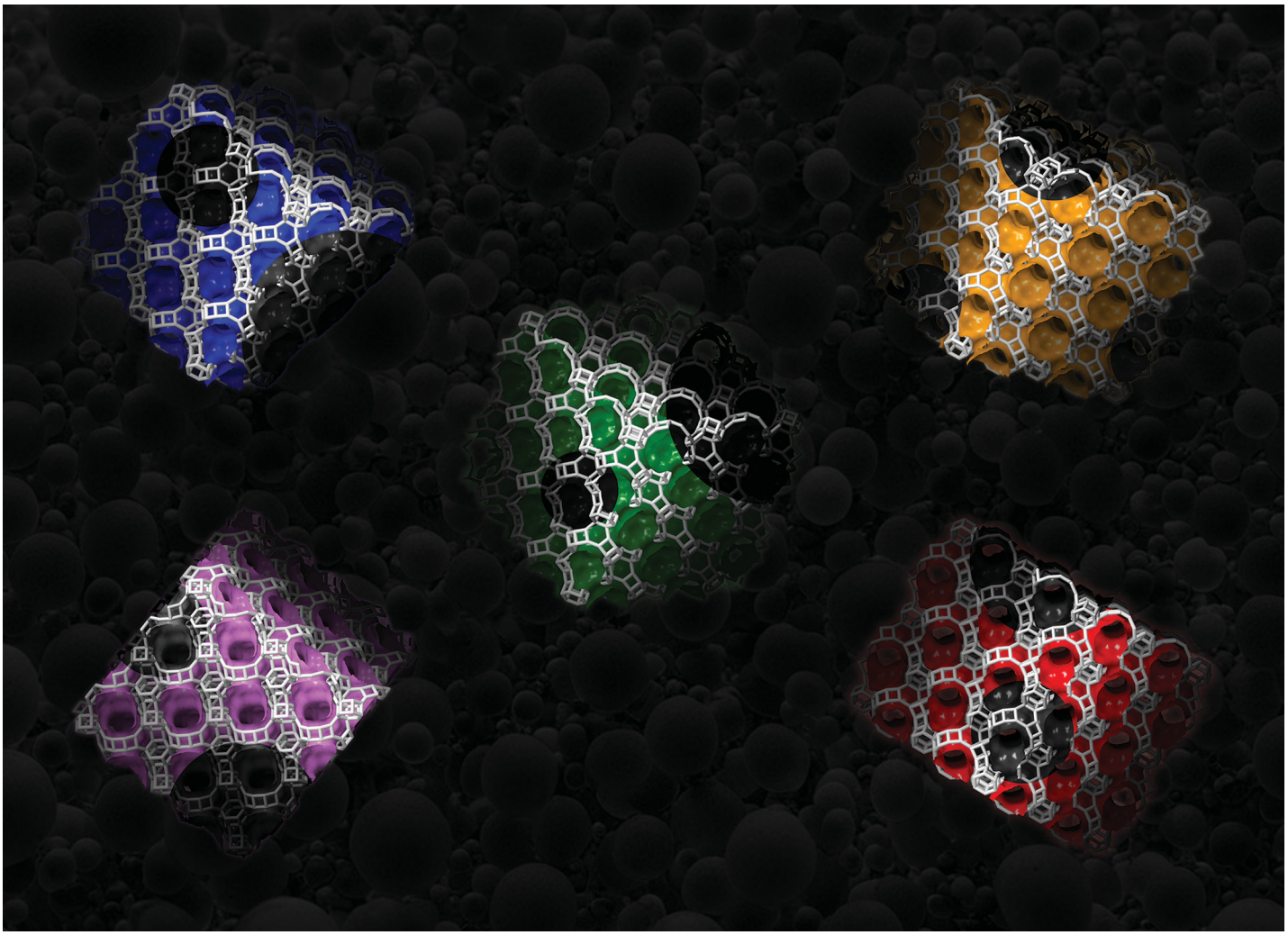

Showcasing research from Professor Shamzhy's laboratory (Department of Physical and Macromolecular Chemistry, Charles University, Prague, Czech Republic) and Dr Galarneau's team (Department of Porous and Hybrid Materials, Institute Charles Gerhardt Montpellier, Montpellier, France)

Correlating mesoporosity/acidity with catalytic performances for surfactant-templated mesoporous FAU zeolites

This study shed light on the cumulative effect in change of activity-determining textural and acidic characteristics concurrently altered during the preparation of surfactant-templated hierarchical zeolite catalysts.

As featured in:

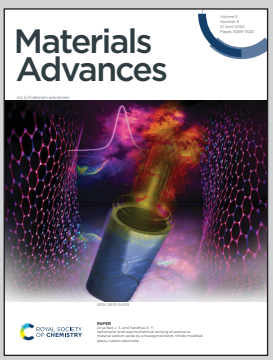

See Mariya Shamzhy, Anne Galarneau *et al.*, *Mater. Adv.*, 2024, **5**, 3207.

ROYAL SOCIETY OF CHEMISTRY

rsc.li/materials-advances

Registered charity number: 207890

Materials Advances

ROYAL SOCIETY OF CHEMISTRY

PAPER

View Article Online
View Journal | View Issue

Cite this: *Mater. Adv.*, 2024, 5, 3207

Correlating mesoporosity/acidity with catalytic performances for surfactant-templated mesoporous FAU zeolites

Yong Zhou, [ab] Anne Galarneau, *[c] Jeremy Rodriguez, [c] Maksym Opanasenko [b] and Mariya Shamzhy *[b]

Hierarchical zeolite catalysts containing additional meso- or macropores have attracted significant interest due to their beneficial performance in various reactions involving bulky molecules. A surfactant-templated post-synthesis of zeolites in basic medium (NaOH) advances from the uniform mesopore size distribution and easy regulation of micro-to-mesopore volume ratio in thus prepared hierarchical zeolites, although their synthesis–acidity–performance relationships remain elusive. In this study, we tackled this problem by designing a series of surfactant-templated hierarchical FAU catalysts with systematically varied textural and acidic characteristics, while assessing their catalytic performance in two model reactions: (1) acid-site-strength insensitive *O*-alkylation of bulky alcohols (1-octadecanol and 1-adamatylmethanol) and (2) acid-site-strength sensitive Friedel–Crafts benzoylation of *p*-xylene. A systematic increase in the NaOH/Si molar ratio in the synthesis from 0.075 to 0.25 decreased the number of strong Brønsted acid sites in hierarchical FAU zeolites, while it increased the concentration of Brønsted acid sites accessible for bulky molecules (up to 67% in hierarchical zeolites *vs.* 21% in the parent FAU zeolite). The development of transport mesopores was shown to positively affect the outcome of the studied reactions independently of the required acid site strength. Although, the optimal interplay between the concentration of strong Brønsted acid sites and their 'accessibility' (*i.e.*, fraction of acid sites accessible to molecules with a kinetic diameter larger than the micropore opening in zeolites) was found to differ for *O*-alkylation of bulky alcohols or Friedel–Crafts benzoylation of *p*-xylene, the possibility of balancing these characteristics in the hierarchical surfactant-templated zeolites was shown by adjusting the NaOH/Si ratio used for their preparation. The results of this study contribute to the understanding of the synthesis–property–performance relationships of surfactant-templated hierarchical zeolite catalysts and provide a guide to tailor the best catalyst for a given reaction.

Received 1st December 2023,
Accepted 1st February 2024

DOI: 10.1039/d3ma01076g

rsc.li/materials-advances

1. Introduction

Zeolites are crystalline microporous aluminosilicates that are applied in important industrial processes because of their large surface area, tunable acidity, high ion-exchange capacity, molecular sieving ability, and high thermal stability. Specifically, zeolites are widely used as catalysts and adsorbents in petroleum refining, fine chemical production, gas separation, *etc.*[1–3] In terms of catalytic applications, the inherent microporous system of zeolites makes them unique shape-selective catalysts, but imposes internal mass transport limitations, specifically in the transformation of bulky molecules.[4–6]

To eliminate diffusion restrictions and to enhance the catalytic activity of zeolites in the transformation of bulky molecules, many synthetic strategies have been developed for the preparation of zeolite catalysts with additional meso- or macroporosity.[7] Traditionally, secondary porosities are introduced into zeolites by post-synthesis demetallation methods, including dealumination,[8] desilication,[9] degermination,[10] and unbiased dealumination/desilication.[11,12] The demetallation approach benefits from a simple and cheap synthesis protocol but produces hierarchical zeolites with mesopores, which are mostly embedded inside the crystals; as a result, the developed mesoporosity provides limited improvement in the transport of reacting molecules to/from the active sites of a catalyst. Hierarchically porous zeolites could also be generated by the

[a] *Research Institute of Interdisciplinary Sciences (RISE) and School of Materials Science & Engineering, Dongguan University of Technology, Dongguan 523808, Guangdong, China*
[b] *Department of Physical and Macromolecular Chemistry, Faculty of Science, Charles University, Hlavova 8, Prague 2 128 43, Czech Republic. E-mail: mariya.shamzhy@natur.cuni.cz*
[c] *ICGM, Univ Montpellier, CNRS, ENSCM, Montpellier, France. E-mail: anne.galarneau@enscm.fr*

addition of hard or soft templates as mesoporogens during direct hydrothermal synthesis.[13–16] The obtained hierarchical zeolites have uniform transport mesopores, although using mesoporogens may hinder the formation of the targeted zeolite phase. In addition, there are several mesoporogen-free methods that are implemented using seed assistance[17,18] and crystallization kinetic regulation,[19–21] thus requiring careful optimization of the synthesis conditions. Hierarchical zeolites have been tested in various catalytic reactions, such as catalytic cracking of hydrocarbons,[22] methanol to hydrocarbons,[23] Fischer–Tropsch synthesis,[24] Friedel–Crafts acylation[25] and alkylation[26,27] reactions among others, in which they showed remarkably improved catalytic activity, selectivity, or stability compared to traditional zeolites.

In addition to the above-mentioned preparation strategies, the surfactant-templating approach was developed for straightforward synthesis of hierarchical zeolites with uniform transport mesopores.[28] This method combines (i) the partial dissolution of the initial zeolite in the basic medium (for example, an aqueous solution of NaOH) in the presence of alkyltrimethylammonium bromide containing 10–22 carbon atoms in the alkyl chain (C_nTAB, n = 10–22), (ii) simultaneous rearrangement of the formed debris around the C_nTAB micelles under hydrothermal conditions and (iii) the removal of surfactant from the formed zeolite–surfactant composite by calcination, which releases the voids with sizes resembling the diameter of micelle and corresponding to the formation of uniform mesopores. In this way, hierarchical zeolites of different types with a uniform size distribution of introduced mesopores were prepared. The advantage of the surfactant-assisted method is that the mesopore-to-micropore volume ratio of the produced zeolites could be varied by a simple adjustment of the basicity in the synthetic mixture. Using this method, Mehlhorn *et al.* synthesized a family of micro–mesoporous FAU zeolites in the presence of octadecyltrimethylammonium surfactant.[29,30] These materials feature uniform mesopores of *ca.* 4 nm diameter, while their textural and acidic properties varied depending on the NaOH/Si ratio used in the reacting mixture. Similarly, Desmurs *et al.* obtained a series of surfactant-templating hierarchical MFI zeolites with variable mesopore volumes by tuning the NaOH/Si ratios in the synthesis gel.[31] They observed that increasing the NaOH/Si ratio resulted in zeolites with a higher mesopore volume but a decreased Brønsted acid site concentration. Among the studied zeolite catalysts, the micro–mesoporous MFI zeolites obtained with NaOH/Si = 0.38 showed the highest yield in the synthesis of 2,4-di-*tert*-butylphenol through alkylation of phenol with *tert*-butyl alcohol, while the micro–mesoporous MFI catalyst prepared using NaOH/Si = 0.50 was the most active in the esterification of benzyl alcohol with hexanoic acid. The obtained results reflect a generally accepted increase in the activity of zeolite catalysts in the transformation or synthesis of bulky molecules with both the 'accessibility' and the number of acid sites,[32,33] although, to our best knowledge, clear synthesis–acidity–performance relationships for surfactant-templating zeolites remain elusive. As both the reactants transport to/from active sites and the characteristics of active sites play an important role in the catalytic transformations over zeolite catalysts, understanding the effect of synthesis conditions on the characteristics of surfactant-templating hierarchical zeolites would open the way to rational optimization of their properties for a given catalytic reaction.

This work aimed at understanding the synthesis–property–performance relationships in surfactant-templating zeolites taking the FAU structural type as a representative example. For that, we have designed and synthesized a series of micro–mesoporous FAU zeolites with systematically varied micropore-to-mesopore volume ratios, comprehensively characterized the textural and acidic properties of the as-prepared catalysts using various techniques (*e.g.*, transmission electron microscopy, X-ray diffraction, nitrogen physisorption, FTIR spectroscopy of adsorbed probe molecules) and related them to the catalytic performance of the designed zeolites in tetrahydropyranylation of bulky alcohols and acylation of *p*-xylene, representing acid-site-strength insensitive and acid-site-strength sensitive reactions, respectively. The obtained results are expected to further the understanding of synthesis–property–performance relationships of surfactant-templated hierarchical zeolite catalysts and to provide a guide for optimizing their properties for a given catalytic reaction.

2. Materials and methods

2.1. Preparations of catalysts

H^+-FAU zeolite with Si/Al = 15 (CBV720) was provided by Zeolyst. A series of micro–mesoporous FAU zeolites with uniform mesopore size distributions and a tunable micro-to-mesopore volume ratio was prepared using a surfactant-templating synthesis method, which we have previously established.[29] Octadecyltrimethylammonium bromide (C_{18}TAB) was chosen as the surfactant to shape the uniform mesopores of *ca.* 4.5 nm in the resultant zeolite catalysts.[34] Typically, the required amount of sodium hydroxide (NaOH) (0.6–2.0 g, corresponding to 0.075–0.25 mol of NaOH per 1 mol of SiO_2, assuming zeolites as pure silica) was dissolved in 180 g of water under ambient conditions. Then, 7.85 g (0.02 mol) of C_{18}TAB was added. After complete surfactant dissolution, 12 g of CBV720 was added to the above solution. After being stirred for 2 hours, the mixture was transferred to a Teflon-lined stainless-steel autoclave and kept at 115 °C for 20 hours under static conditions. The micro–mesoporous FAU zeolite products were filtered and thoroughly washed with water, then dried at 80 °C for 12 hours and calcined in air at 550 °C for 8 hours. The calcined micro–mesoporous FAU zeolites were then ion-exchanged with a 0.1 mol L^{-1} NH_4NO_3/ethanol solution at 90 °C for 1 hour three times to obtain the NH_4^+ form of the materials. A calcination at 450 °C for 6 hours was then applied to decompose NH_4^+ into NH_3 and hence produce the H^+ form of the catalysts. The obtained catalysts were denoted as NaOH/Si-n (n = 0.075, 0.095, 0.125 and 0.25, referring to the NaOH/Si molar ratios used for catalyst preparation).

2.2. Characterization studies of catalysts

Transmission electron micrograph (TEM) images were obtained using a JEOL 1200 EX2 microscope operating at 100 kV at "Plateau Technique du Pole Chimie Balard Montpellier".

Powder X-ray diffraction (XRD) patterns of the catalysts were collected using a Bruker D8 Advance diffractometer using Cu Kα radiation (30 kV, 40 mA). The textual properties of the catalysts were determined by nitrogen sorption isotherms at −196 °C using an ASAP 2020 Micromeritics apparatus. 100 mg of materials were outgassed under vacuum at 350 °C for 6 h prior to nitrogen sorption analysis. The specific surface area was determined using the BET method. The relative pressure range to use the BET equation $(p/p_0)/[V(1 - p/p_0)] = f(p/p_0)$ was determined using the superior limit given by the maximum of the Rouquerol curve $V(1 - p/p_0) = f(p/p_0)$.[35] The mesopore pore-size distribution was evaluated using the Broekhoff and de Boer (BdB) method[36] at the inflection point of the desorption step, while the values of micropore and mesopore volumes and surfaces were determined by the corrected *t*-plot method.[30,37] As a comparison and to establish pore size distribution for micro- and mesopores, pore diameters were also calculated by the NLDFT method with software SAIEUS of Micromeritics (model: zeolites (H-form)-N2-77, NLDFT (cylindrical)) using the desorption branch of the isotherms.

Concentrations of Lewis (C_{LAS}) and Brønsted (C_{BAS}) acid sites were determined after adsorption of pyridine (Py) by Fourier-transform infrared spectroscopy (FTIR) on Nicolet iS50 FTIR with MCT/B detector. The zeolites were pressed into self-supporting wafers with a density of 8–12 mg cm^{-2} and activated *in situ* at 450 °C for 4 h. Pyridine adsorption was carried out at 150 °C for 20 minutes at 600–800 Pa partial pressure, followed by desorption for 20 minutes at 150, 250, 350 or 450 °C. Before adsorption, pyridine was degassed by freezing and thawing cycles. All spectra were recorded with a resolution of 4 cm^{-1} by collecting 128 scans for a single spectrum at room temperature. Spectra were calculated at a wafer density of 10 mg cm^{-2}. The total concentration of BAS ($C_{BAS\text{-}Py}$) and LAS ($C_{LAS\text{-}Py}$) was evaluated from the integral intensities of the absorption bands at 1545 cm^{-1} 1455 cm^{-1} after pyridine desorption at 150 °C ($A_{1545}^{150\,°C}$ and $A_{1545}^{150\,°C}$) using molar absorption coefficients, ε_{1545} = 1.54 cm μmol^{-1}, and ε_{1545} = 1.71 cm μmol^{-1} [38] according to the following equations:

$$C_{BAS} = \frac{A_{1545}^{150\,°C} \cdot S}{m \cdot \varepsilon_{1545}} \left[\mu mol\, mg^{-1}\right] \quad (1)$$

$$C_{LAS} = \frac{A_{1455}^{150°C} \cdot S}{m \cdot \varepsilon_{1455}} \left[\mu mol\, mg^{-1}\right] \quad (2)$$

where S is area of the wafer (cm^2) and m is the weight of the wafer (mg).[39]

To estimate the fraction of strong Lewis and Brønsted acid sites, the intensity of the characteristic bands at 450 °C was related to those at 150 °C as follows:

$$BAS_{strong} = \frac{A_{1545}^{450\,°C}}{A_{1545}^{150\,°C}} \times 100\ [\%] \quad (3)$$

$$LAS_{strong} = \frac{A_{1455}^{450\,°C}}{A_{1455}^{150\,°C}} \times 100\ [\%] \quad (4)$$

A relatively large probe molecule 2,6-di-*tert*-butylpyridine (DTBP) with a kinetic diameter of 0.79 nm[40] was used to determine the 'accessibility' of acid sites within prepared zeolites.[41] DTBP adsorption took place at 150 °C at equilibrium probe vapour pressure for 15 minutes. Desorption proceeded at the same temperature for 1 hour, followed by the collection of spectra at room temperature. Molar absorption coefficient from ref. 42 was used for the evaluation of C_{BAS} accessible for DTBP using the integral intensity of the absorption band at *ca.* 3360 cm^{-1}.

2.3. Catalytic tests

The catalytic performances of micro–mesoporous FAU zeolites were evaluated in the liquid-phase tetrahydropyranylation and acylation reactions. Both reactions were conducted under atmospheric pressure on a multi-experimental workstation StarFish™. Before catalytic tests, 50 mg of the zeolite sample was activated at 450 °C for 1.5 hours to evacuate possible guest molecules that may bind to the acid sites in the zeolite pores. The liquid-phase tetrahydropyranylation reaction was performed at 65 °C. Typically, 3,4-dihydro-2*H*-pyran (DHP, 10 mL), internal standard (mesitylene, 0.4 g), and catalyst (50 mg) were added to a three-neck flask equipped with a thermometer and a condenser. Alcohol (2 mmol of 1-octadecanol or 1-adamantanemethanol) was added to the flask when the required temperature was reached. The surfactant-templated zeolite catalysts were studied under conditions providing high conversion values relevant for practical application, but not allowing us to use the obtained results for the kinetic analysis. Therefore, the catalytic performance of surfactant-templated zeolites in THP reaction of bulky alcohols was analyzed focusing on the impact of mass transport limitations rather than being discussed within the context of kinetic analysis.

The liquid-phase acylation reaction was performed at 130 °C. *p*-Xylene (5 mL), internal standard (dodecane, 0.25 g), and the catalyst (50 mg) were added to a three-neck flask. Benzoyl chloride (5 mmol) was added to the flask when the required temperature was reached.

The samples of the reaction mixture were taken periodically and analyzed using a gas chromatography instrument (Agilent 7890B) equipped with a HP-5 column (30 m × 0.32 mm × 0.25 μm) and an FID detector.

Conversion (X), yield (Y) and selectivity (S) were calculated according to the following equations:

$$X = [(n(\text{reactant})_0 - n(\text{reactant})_t)/n(\text{reactant})_0] \times 100\,[\%] \quad (5)$$

$$Y = [n(\text{product})_t/n(\text{reactant})_0] \times 100\,[\%] \quad (6)$$

$$S = [Y/X] \times 100\,[\%] \quad (7)$$

where $n(\text{reactant})_0$ and $n(\text{reactant})_t$ are the amounts of the reactant in the reaction mixture initially and after a specific time t; $n(\text{product})_t$ is the amount of the product formed after a specific time t. n(reactant) and n(product) values in eqn (5) and

(6) were determined based on the internal standard calibration method, using commercially available 1-octadecanol (99%, Sigma Aldrich), 1-adamantanemethanol (99%, Fisher Scientific) and benzoyl chloride (≥99%, Sigma Aldrich). The amounts of commercially unavailable products, *n*(product), were estimated using the concept of effective carbon number.[43]

The activity of zeolite catalyst was assessed by their initial reaction rate per acid site. The initial reaction rate was calculated as a slope to the graph of product concentration against the reaction time at t = 0 and then normalized to the total concentration of BAS and LAS as determined by FTIR-Py after desorption of the probe molecule at 150 °C (R_{total}) or to the concentration of strong BAS and LAS as determined by FTIR-Py after desorption of the probe molecule at 450 °C (R_{strong}).

3. Results and discussion

3.1. Physicochemical properties of FAU zeolites prepared *via* a surfactant-templating method

The structural properties of the hierarchical FAU zeolites NaOH/Si-*n* obtained by the surfactant-templating method in basic medium with variable NaOH/Si ratios were studied using TEM, XRD, and nitrogen physisorption. TEM images show the decrease in the size of the crystalline zeolite nanodomains in NaOH/Si-*n* (n = 0.075; 0.095; 0.125) compared to CBV720 (Fig. 1). For the NaOH/Si-0.25 sample obtained with the highest base concentration, the crystalline domains almost completely disappeared and a hexagonal structure ordered on a mesoscale, similar to MCM-41,[44,45] could be seen in majority.

In agreement with the TEM results, the XRD patterns of the initial CBV720 and NaOH/Si-*n* (n = 0.075; 0.095; 0.125) samples clearly show intensive Bragg peaks characteristic of FAU zeolite (*e.g.*, 111, 220, 311, 331 in Fig. 2a), while NaOH/Si-0.25 demonstrated a remarkable decrease in the intensity of these diffraction lines.[46] In particular, the intensities of the peaks attributed to FAU zeolite decreased in the following order CBV720 > NaOH/Si-0.075 ≈ NaOH/Si-0.095 > NaOH/Si-0.125 ≫ NaOH/Si-0.25, which suggested a higher depletion of zeolite phase for the samples synthesized at higher NaOH/Si. Another characteristic feature seen in XRD patterns of NaOH/Si-*n* samples is the appearance of the low-angle 2θ peak at around 2° (Fig. 2b), indicating the mesoscale ordering.[47]

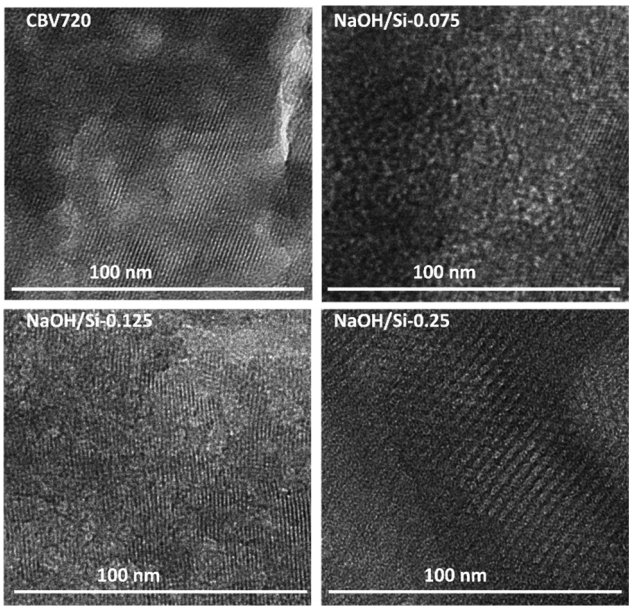

Fig. 1 TEM images of FAU-Y (CBV720) and micro–mesoporous FAU zeolites (NaOH/Si-*n*).

The nitrogen sorption isotherms of NaOH/Si-*n* zeolites exhibit a combined type *I* + *IV*, characteristic of materials possessing both micro- and mesopores (Fig. 2c). A steep increase in the adsorbed amount in the range of $0.35 < p/p_0 < 0.55$ characteristic of all NaOH/Si-*n* materials suggested a narrow mesopore size distribution[29] centered at 4.0–4.5 nm (as evaluated by the BdB and NLDFT methods, Table 1). Both mesopore-to-micropore volume ratios and surface areas of hierarchical surfactant-templated NaOH/Si-*n* zeolites increased as the n value grew (Table 1). Notably, all NaOH/Si-*n* samples with $n < 0.25$ possess a similar external surface area (50 $m^2 g^{-1}$) and high C_{BET} parameters (578–815) as expected for materials containing micropores. On the contrary, NaOH/Si-0.25 has a larger external surface area (90 $m^2 g^{-1}$) (Table 1), but C_{BET} as low as 125. The results of physisorption validate NaOH/Si-0.25 as close to a pure mesoporous catalyst, similar to the Al-MCM-41-type material, although containing some strong Brønsted acid sites (*vide infra*).

The type, concentration, and strength of acid sites in the designed hierarchical FAU zeolites were determined by FTIR spectroscopy using probe molecules of different kinetic diameters: pyridine (0.54 nm) and 2,6-di-*tert*-butylpyridine (0.79 nm). The spectra of activated CBV720 and NaOH/Si-*n* samples showed the bands corresponding to the Brønsted acid sites (BAS) in the OH vibration region (3631 and 3565 cm^{-1}, Fig. 3a), while the adsorption of pyridine completely removed these bands, suggesting the 100% 'accessibility' of BAS in all the studied materials for the pyridine probe. Analysis of the characteristic absorption bands in the FTIR-Py spectra revealed a remarkable decrease in the concentration of BAS (by 35–68%) and less severe drop in the number of Lewis acid sites (by 11–21%) in micro–mesoporous NaOH/Si-*n* zeolites (n = 0.075; 0.095; 0.125) compared to the initial CBV720 (Fig. 3c and Table 2). Among NaOH/Si-*n* samples, the zeolite-poor mesostructured NaOH/Si-0.25 showed the highest drop in BAS concentration by 78%, but increased number of Lewis acid sites. Notably, zeolite-poor mesostructured NaOH/Si-0.25 possessed significantly lower part of strong BAS (Fig. 3b), while the micro–mesoporous FAU NaOH/Si-*n* samples (n = 0.075; 0.095; 0.125) prepared with lower NaOH/Si ratios contained a similar fraction of strong Brønsted and Lewis acid sites retaining pyridine at 450 °C as the initial CBV720 zeolite.

At the same time, compared to the initial CBV720 sample, the fraction of Brønsted acid sites accessible for DTBP increases greatly for NaOH/Si-*n* (n = 0.095; 0.125; 0.25) (44–67%, Table 2), while NaOH/Si-0.075 prepared with the lowest NaOH/Si ratio showed just a slight increase in BAS 'accessibility' compared to

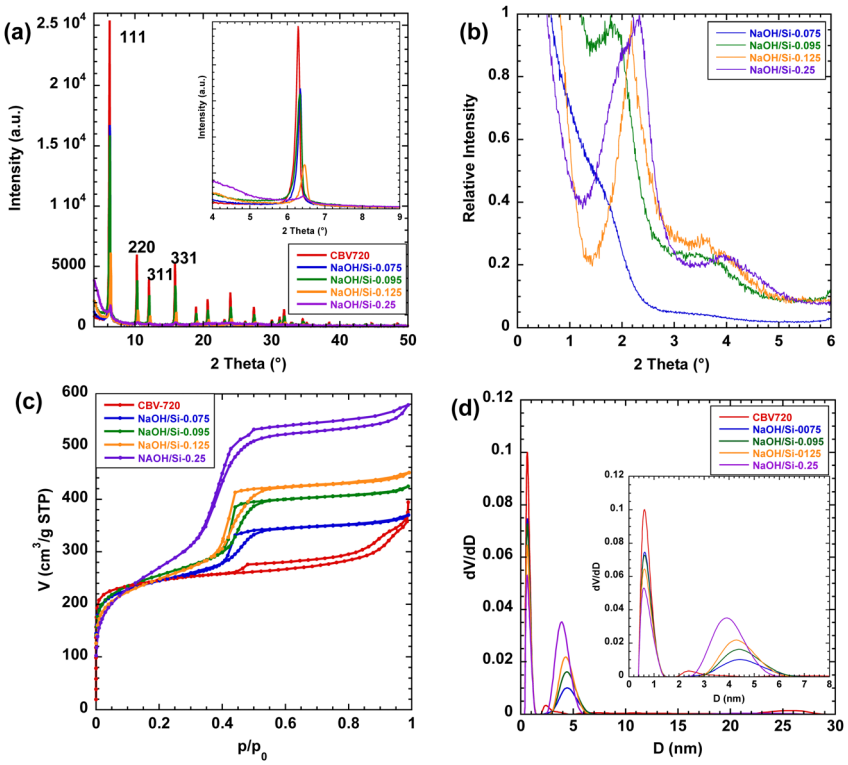

Fig. 2 Powder XRD patterns (a) and (b), N_2 sorption isotherms at 77 K (c) and NLDFT pore size distribution (d) of FAU-Y (CBV720) and micro–mesoporous FAU zeolites (NaOH/Si-*n*).

Table 1 Textural properties of FAU zeolites

Catalyst	Relative pressure region[a]	S_{BET} ($m^2\ g^{-1}$)	C_{BET}	S_{mic}[b] ($m^2\ g^{-1}$)	S_{mes}[b] ($m^2\ g^{-1}$)	S_{ext}[b] ($m^2\ g^{-1}$)	V_{tot}[b] (mL g^{-1})	V_{mic}[b] (mL g^{-1})	V_{mes}[b] (mL g^{-1})	D_{BdB} (nm)	D_{NLDFT}[e] (nm)
CBV720	0.001–0.043	946	2304	832	0[d]	99	0.37	0.37[c]	0[d]	22[d]	25
NaOH/Si-0.075	0.010–0.075	910	815	581	280	49	0.53	0.32[c]	0.21	4.3	4.5
NaOH/Si-0.095	0.010–0.100	934	578	493	390	51	0.62	0.28[c]	0.34	4.3	4.4
NaOH/Si-0.125	0.019–0.126	879	707	349	477	53	0.65	0.22	0.44	4.2	4.3
NaOH/Si-0.25	0.040–0.275	969	123	44	835	90	0.81	0.02	0.78	4.0	3.9

[a] Relative pressure domain for S_{BET} calculation obtained following Rouquerol criteria.[37] [b] Determined by the corrected *t*-plot method.[37] [c] V_{mic} supercage = 0.28 mL g^{-1}; supercages could remain in these FAU zeolites. [d] Some mesopores are present in the initial dealuminated FAU-Y (CBV720), as observed by TEM, but they are mainly embedded inside the crystals without connections to the exterior of the crystals, as revealed by the horizontal hysteresis characteristic of cavitation phenomenon in the nitrogen sorption isotherm. However, a small fraction of mesopores is connected to the exterior of the crystals, as observed by the vertical hysteresis at $p/p_0 \sim 0.90$, corresponding to mesopores of 22 nm diameter and a mesopore volume of ~0.09 mL g^{-1}. These very large mesopores are not counted in the corrected *t*-plot method, and the external surface area can be counted as the mesopore surface area for CBV720. [e] Pore diameters calculated by the NLDFT method with software SAIEUS of Micromeritics model: zeolites (H-form)-N2-77, NLDFT (cylindrical) are given for comparison. Micropore diameters calculated by this method were 0.63 nm for FAU-Y (CBV720), NaOH/Si-0.075 and NaOH/Si-0.095, and 0.61 nm for NaOH/Si-0.125 and NaOH/Si-0.25. FAU-Y features windows of 0.74 nm and cavities of 1.3 nm, and the chosen NLDFT model gives an equivalent cylindrical diameter of 0.63 nm.

CBV720 (29%). This result is in line with a decrease in the size of the crystalline zeolite domains of the FAU samples confirmed by TEM (Fig. 1) and an XRD (Fig. 2) and increase in the fraction of mesopores confirmed by nitrogen physisorption (Table 1).

3.2. Catalytic performances of micro–mesoporous FAU zeolites

The results of the above comprehensive characterization studies for a series of hierarchical surfactant-templated FAU zeolites indicate a systematic increase in the volume and surface area of mesopores, a decrease in the volume and surface area of micropores, and a decrease in the number of Brønsted acid sites with an increase in the NaOH/Si ratio used for their synthesis (Fig. 4).

The decrease in BAS concentration appears to follow the decrease in the micropore surface area (Fig. 4) (and a related increase in the mesopore surface area). To understand the influence of the collaborative change in textural properties (facilitating the transport of reacting molecules) and acidic

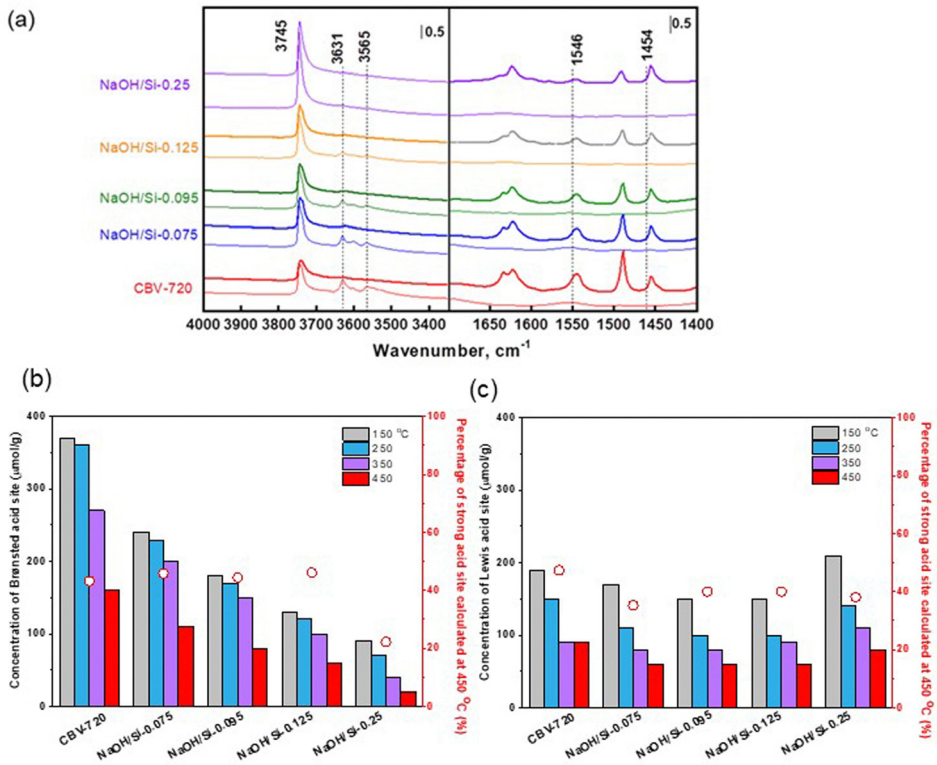

Fig. 3 (a) FTIR spectra of FAU-Y (CBV720) and micro–mesoporous FAU zeolites (NaOH/Si-*n*) in the OH vibration region (left) and the pyridine-ring vibration region (right) before (thin lines) and after (thick lines) pyridine adsorption. Absolute total concentrations (bars) and relative concentrations of strong acid centers (circles) for (b) BAS and (c) LAS, determined by FTIR spectroscopy of adsorbed pyridine.

Table 2 Acidic properties of FAU-Y (CBV720) and micro–mesoporous FAU zeolites determined by FTIR using pyridine (Py) and 2,6-di-*tert*-butylpyridine (DTBP) as molecular probes

	Pyridine (mmol g^{-1})			DTBP (mmol g^{-1})
Catalyst	$C_{BAS\text{-}Py}$	$C_{LAS\text{-}Py}$	LAS/BAS	$C_{BAS\text{-}DTBP}$
CBV720	0.37	0.19	0.5	0.08 (21%)[b]
NaOH/Si-0.075	0.24 (−35%)[a]	0.17 (−11%)[a]	0.7	0.07 (29%)[b]
NaOH/Si-0.095	0.18 (−51%)[a]	0.15 (−21%)[a]	0.8	0.08 (44%)[b]
NaOH/Si-0.125	0.13 (−68%)[a]	0.15 (−21%)[a]	1.2	0.07 (54%)[b]
NaOH/Si-0.25	0.09 (−76%)[a]	0.21 (+11%)[a]	2.3	0.06 (67%)[b]

[a] The values in brackets show the % change in the concentration of acid sites in NaOH/Si-*n* samples compared to the initial CBV-720. [b] The values in brackets are the ratio of $C_{BAS\text{-}DTBP}$ to $C_{BAS\text{-}Py}$, indicating the % of BAS accessible for DTBP.

characteristics (decreasing the number of catalytically active sites) in surfactant-templating hierarchical zeolites on their catalytic performance, the designed series of NaOH/Si-*n* catalysts were tested in model reactions with different requirements to the strength of acid sites: (1) *O*-alkylation of alcohols which proceeds on both strong acid sites and acid centers of relatively low strength; and (2) Friedel–Crafts acylation, requiring relatively strong acid sites.

3.2.1. Tetrahydropyranylation of alcohols with 3,4-dihydro-2*H*-pyran. Hierarchical NaOH/Si-*n* zeolites with systematically varied textural properties were first investigated in acid-site-strength-insensitive *O*-alkylation of two bulky alcohols (1-octadecanol and 1-adamantanemethanol) with 3,4-dihydro-2*H*-pyran (Fig. 5a). According to the literature, both Brønsted and Lewis acid sites can catalyze this reaction, but strong BAS are more active than LAS.[48–50] In addition, the diffusion of reactants in zeolite catalysts was reported as the rate-determining step.[50] Therefore, hierarchical zeolites with transport mesopores or macropores that facilitate the diffusion of reactants are considered the best candidates for the tetrahydropyranylation reaction.[50–52] In our study, only targeted tetrahydropyranyl ethers were detected as products (*i.e.*, selectivity >99%) in the *O*-alkylation of both alcohols over the investigated catalysts, initial CBV720 or hierarchical NaOH/Si-*n*. Over CBV720, the conversion of 1-octadecanol gradually reached a plateau at ∼45% after 120 min (Fig. 5). In turn, all surfactant-templated micro–mesoporous FAU NaOH/Si-*n* materials showed higher 1-octadecanol conversion of 72–87% achieved after 60 min. Specifically, the activity of micro–mesoporous FAU catalysts in *O*-alkylation of 1-octadecanol increased in the order of NaOH/Si-0.075 (77% yield after 60 min) < NaOH/Si-0.095 (80%) < NaOH/Si-0.125 (87%), which is consistent with facilitation of the transport of reacting molecules as the total pore volume and the mesopore volume increase. The mesostructured sample NaOH/Si-0.25 with the highest mesopore volume-to-micropore volume ratio (Table 1) was the only exception to this trend. While outperforming the initial CBV720 catalyst, NaOH/Si-0.25 showed a slightly lower 1-octadecanol conversion (72% after 60 min) compared to other studied hierarchical zeolites. This result may be related to

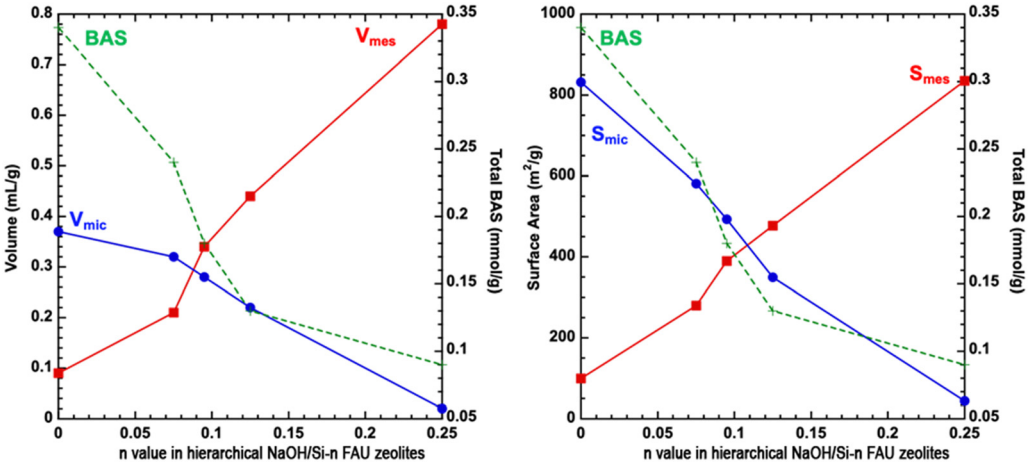

Fig. 4 Evolution of micro- and mesopore volume and surface area in hierarchical FAU zeolites prepared with different NaOH/Si ratios. Comparison with the evolution of the number of Brønsted acid sites (BAS).

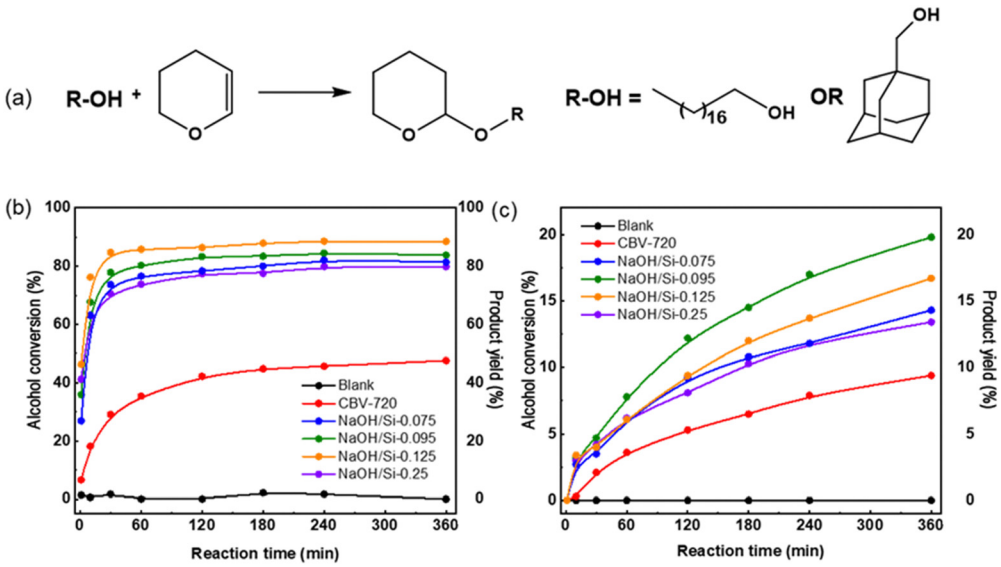

Fig. 5 (a) Schematic representation of the studied *O*-alkylation reaction. Alcohol conversions (equivalent to product yields) in tetrahydropyranylation of (b) 1-octadecanol and (c) 1-adamantanemethanol with 3,4-dihydro-2*H*-pyran over FAU-Y (CBV720) and micro–mesoporous FAU zeolites (NaOH/Si-*n*) as a function of reaction time. Reaction conditions: 50 mg of zeolite catalyst, 10 mL of 3,4-dihydro-2*H*-pyran as both solvent and reactant, 2 mmol of 1-octadecanol or 1-adamantanemethanol, and 0.4 g of mesitylene as internal standard, 65 °C.

the dominating concentration of less active Lewis acid sites in NaOH/Si-0.25 (LAS/BAS = 2.3) compared to NaOH/Si-*n* with $n < 0.25$ (LAS/BAS = 0.7–1.2, Table 2).

Similarly, in the *O*-alkylation of bulkier 1-adamantanemethanol, all surfactant-templated micro–mesoporous FAU zeolites outperformed the initial CBV720 (1-adamantanemethanol conversion after 360 min of 13–21% for NaOH/Si-*n* *vs.* 8% for initial FAU-Y, Fig. 5c). The highest conversion of 1-adamantanemethanol was observed over NaOH/Si-0.95 prepared at a medium NaOH/Si molar ratio. Compared to NaOH/Si-0.95, less active NaOH/Si-*n* showed a smaller mesopore volume ($n = 0.075$, Fig. 4) or a lower concentration of Brønsted acid sites ($n = 0.125$ and $n = 0.25$, Fig. 4).

Incomplete conversion of both alcohols even for the most active FAU NaOH/Si-*n* catalysts can be partially related to the reversible character of tetrahydropyranylation reaction[53] and catalyst deactivation. The generally lower conversion reached for 1-adamantanemethanol compared to 1-octadecanol over the studied zeolite catalysts may be explained by the difference in the reactivity of two alcohols, including diffusion restrictions. While a rigid adamantyl alkyl substituent provides permanent bulkiness to the respective reactant molecule, the long-chain 1-octadecanol molecule can exist in a linear or elongated conformation. This conformational flexibility is assumed to increase the probability of transformation of 1-octadecanol at the active sites located at the micropore entrances in comparison

to 1-adamantanemethanol, while the acid sites at the external surface are considered accessible for both alcohol reactants.

To provide more insight into the acidity–activity relationships for *O*-alkylation of bulky alcohols over surfactant-templated micro–mesoporous FAU zeolites, we further estimated the activity of the catalysts. Specifically, we estimated the catalysts' activity in terms of initial reaction rates (R) normalized per acid site.[54] This metric represents the number of reactant molecules converted per acid site per hour and was calculated based on the slope to the graph of products concentration against the reaction time at $t = 0$. This calculation was made under the assumption that catalyst deactivation at this initial point was negligible. In addition, although the initial reaction rate may vary depending on experimental conditions, such as the initial concentrations of reagents, it was considered a reliable descriptor of the studied catalysts as the catalytic experiments were conducted under identical conditions. Thus evaluated initial rate values were separately analyzed for acid sites that retain pyridine at 150 °C (R_{total}, Fig. 6a and b) and for the strongest acid sites that retain pyridine at 450 °C (R_{strong}, Fig. 6c and d). These activity indicators enable a direct comparison of catalysts containing different concentrations of acid sites and differing in their strength.

For both 1-octadecanol and 1-adamantanemethanol, R_{total} values increased in the order of CBV720 < NaOH/Si-0.075 < NaOH/Si-0.095 < NaOH/Si-0.25 < NaOH/Si-0.125 (Fig. 5a and c). Except for NaOH/Si-0.25 (showing a markedly lower fraction of strong acid sites compared to other catalysts studied), the increase in catalyst activity corresponds to the increase in the volume of transport mesopores (Fig. 4). In turn, the obtained R_{strong} values suggest a similar intrinsic activity of acid sites with similar strength to NaOH/Si-0.125 and NaOH/Si-0.25 with the highest 'accessibility' of acid centers showing similar R_{strong} (Fig. 5b and d).

A comparison of NaOH/Si-*n* and CBV720 catalysts in the acid-site-strength insensitive tetrahydropyrahylation of 1-octadecanol and 1-adamantanemethanol revealed a positive effect of the development of transport mesopores in hierarchical surfactant-templated FAU zeolites for either conformationally flexible or rigid bulky alcohols, the trend, which is not compromised by either increase in LAS/BAS ratio or decrease in the total concentration of acid sites.

3.2.2. Acylation of *p*-xylene with benzoyl chloride. To further investigate the effect of the development of transport mesopores combined with a decrease in the concentration of BAS with increasing NaOH/Si ratio in surfactant-templating synthesis of hierarchical zeolites, we tested the designed

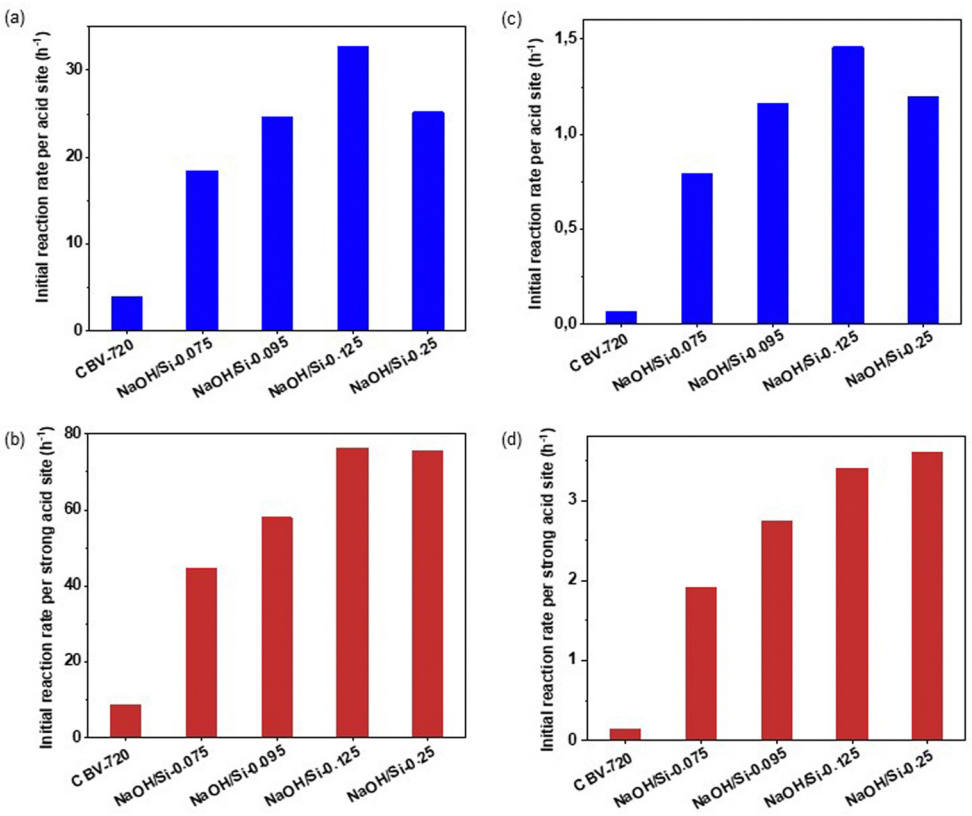

Fig. 6 Initial reaction rates per acid site values in the tetrahydropyranylation of 1-octadecanol (a) and (b) and 1-adamantanemethanol (c) and (d) with 3,4-dihydro-2*H*-pyran on FAU-Y (CBV720) and micro–mesoporous FAU zeolites (NaOH/Si-*n*). (a) and (c) Rates calculated based on the total concentration of acid sites (LAS + BAS) determined by FTIR-Py at 150 °C and (b) and (d) rates calculated based on the concentration of strong acid sites (LAS + BAS) determined by FTIR-Py at 450 °C. Reaction conditions: 50 mg of zeolite catalyst, 10 mL of 3,4-dihydro-2*H*-pyran as solvent and reactant, 2 mmol of 1-octadecanol or 1-adamantanemethanol, 0.4 g of mesitylene as internal standard, 65 °C, and 6 hours.

micro–mesoporous FAU catalysts in the acylation of *p*-xylene with benzoyl chloride, requiring relatively strong acid sites. Zeolites with medium Brønsted acid sites (*e.g.*, Ga-associated BAS) and strong Brønsted acid sites (*e.g.*, Al-associated BAS) were reported to catalyze the formation of targeted 2,5-dimethylbenzophenone (pathway 1 in Fig. 7a) by facilitating the formation of a benzoic ion intermediate, which interacts with arene to offer the desired product.[55] In contrast, zeolites with weak Brønsted acid sites (*e.g.*, B-associated BAS) showed the preferential formation of undesired benzoyl anhydride due to side reactions of benzoyl chloride hydrolysis (pathway 2 in Fig. 7a).[55,56] An interesting feature of heterogeneously catalyzed Friedel–Crafts acylation reaction is the phenomenon of product inhibition related to strong adsorption of the ketonic products on the Lewis acid sites.[55,57]

Over FAU-Y (CBV720) and micro–mesoporous FAU zeolites (NaOH/Si-*n*) catalysts, 2,5-dimethylbenzophenone was formed as the main product (selectivity > 80%). The formation of the undesired benzoic anhydride product increased with decreasing concentration of strong acid sites according to previous reports.[55,56] At 15% benzoyl chloride conversion, the selectivity in the undesired benzoic anhydride product increased in the following order: NaOH/Si-0.075 (1%) < NaOH/Si-0.095 (5%) < NaOH/Si-0.125 (7%) < NaOH/Si-0.25 (20%). Among hierarchical FAU zeolites, only NaOH/Si-0.075 with the highest fraction of the remaining zeolite phase and the highest concentration of Brønsted acid sites outperformed the initial CBV720 in terms of benzoyl chloride conversion (Fig. 7b) and yield of 2,5-dimethylbenzophenone (Fig. 8).

NaOH/Si-*n* (n = 0.095, 0.0125 and 0.25) catalysts with lower concentration of BAS and higher LAS/BAS ratio showed lower yields of 2,5-dimethylbenzophenone in comparison to the initial CBV720 zeolite (Fig. 8). As mentioned above, the acylation reaction is generally promoted by medium and strong acid sites on zeolite catalysts, while the probability of "product inhibition" increases with the LAS/BAS ratio.[55,57] Therefore, the enhanced benzoyl chloride conversion and target product selectivity over NaOH/Si-0.075 should be attributed to the higher concentration of strong acid sites, lower LAS/BAS ratio in this hierarchical zeolite in comparison to NaOH/Si-*n* (n = 0.095, 0.0125 and 0.25) and better transport of reagents compared to CBV720. R_{total} numbers calculated based on the total concentration of Brønsted and Lewis acid sites in hierarchical zeolites showed an interesting trend, suggesting

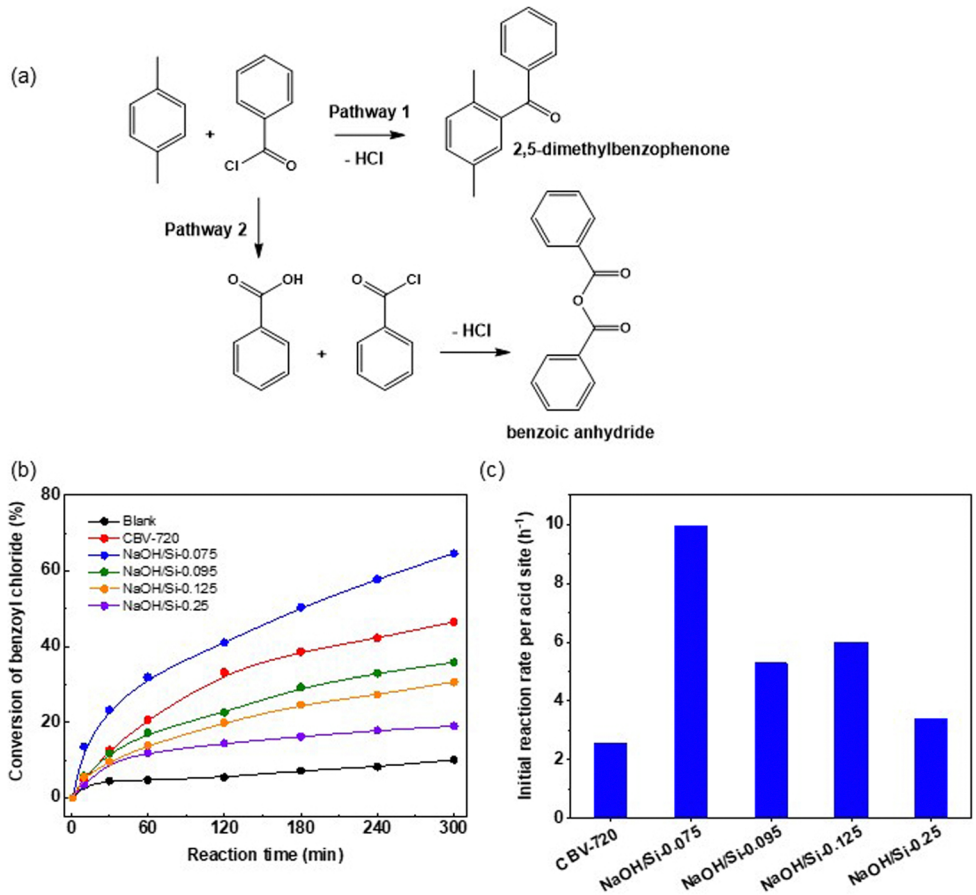

Fig. 7 (a) Schematic representation of the reaction of *p*-xylene acylation. (b) Conversion of benzoyl chloride over FAU-Y (CBV720) and micro–mesoporous FAU zeolites (NaOH/Si-*n*) as a function of reaction time. (c) Initial reaction rates per acid site values in the acylation of *p*-xylene with benzoyl chloride over FAU-Y (CBV720) and micro–mesoporous FAU zeolites (NaOH/Si-*n*). Reaction conditions: 50 mg of zeolite catalyst, 5 mL of *p*-xylene as both solvent and reactant, 5 mmol of benzoyl chloride, 0.25 g of dodecane as internal standard, and 130 °C.

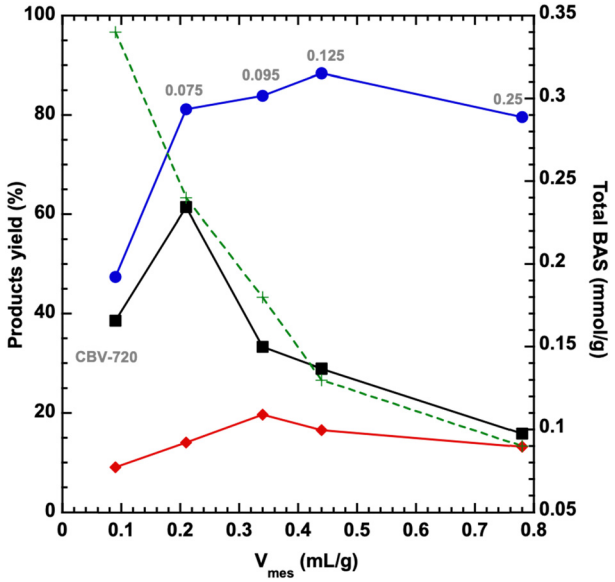

Fig. 8 Yield of the targeted products for *O*-alkylation of 1-octadecanol (blue), *O*-alkylation of 1-adamantanemethanol (red) and the Friedel–Crafts acylation of *p*-xylene with benzoyl chloride (black) as a function of mesopore volume for the initial CBV720 zeolite and hierarchical FAU NaOH/Si-*n* (*n* values are shown in grey). The change in the total number of Brønsted acid sites for the studied catalyst is shown as a function of their mesopore volume in green.

the importance of the acid site type, rather than their 'accessibility' for the activity of a catalyst in the benzoylation of *p*-xylene. Specifically, after a notable increase in the R_{total} value for NaOH/Si-0.075 *vs.* initial CBV720, the R_{total} decreased in NaOH/Si-0.95 and was similar to NaOH/Si-*n* (n = 0.125; 0.25) despite an increase in the 'accessibility' of acid sites (Fig. 7c).

A comparison of NaOH/Si-*n* and CBV720 catalysts in Friedel–Crafts acylation of *p*-xylene with benzoyl chloride revealed that the best hierarchical zeolite catalyst for this reaction maintains a high concentration of BAS together with the addition of mesopores, which is in line with the crucial role of acid site type and strength for the Friedel–Crafts acylation reaction.

4. Conclusions

This study aimed to shed light on the cumulative effect in the change of activity-determining textural and acidic characteristics concurrently altered during the preparation of surfactant-templated hierarchical zeolites. For this, a series of surfactant-templated hierarchical FAU catalysts with systematically varied textural and acidic characteristics was designed, while their catalytic performance was assessed in two model reactions: (1) acid-site-strength insensitive *O*-alkylation of bulky alcohols (1-octadecanol and 1-adamatylmethanol) and (2) acid-site-strength sensitive Friedel–Crafts benzoylation of *p*-xylene.

A systematic increase in the NaOH/Si ratio from 0.075 to 0.25 used for the surfactant-templating synthesis of hierarchical FAU zeolites led to a progressive decrease in the size of crystalline FAU zeolite domains resulting in: (1) an increase in the mesopore volume from 0.21 to 0.78 mL g^{-1}; (2) a decrease in the micropore volume from 0.32 to 0.02 mL g^{-1}; (3) an increase in the fraction of Brønsted acid sites accessible for 2,6-di-*tert*-butylpyridine from 29% to 67%; but (4) a decrease in the concentration of Brønsted acid sites characteristic of a zeolite phase.

A comparison of NaOH/Si-*n* and CBV720 catalysts in Friedel–Crafts acylation of *p*-xylene with benzoyl chloride and in the tetrahydropyrahylation of 1-octadecanol and 1-adamantanemethanol suggests that the development of transport mesopores in hierarchical surfactant-templated FAU zeolites positively affected their performance in either acid-site-strength sensitive and acid-site-strength insensitive reactions. However, the optimised micro–mesoporous zeolite catalysts are different for the reactions studied (Fig. 8). For the *O*-alkylation reaction, which requires moderate acidity, hierarchical zeolites prepared in a NaOH/Si ratio of 0.095 or 0.125 and featuring highly developed mesoporosity (*e.g.*, mesopore volume >0.33 mL g^{-1}) were the most active catalysts, despite a drop in the concentration of strong BAS. In turn, for catalytic reactions that need strong acid sites, such as acylation, the best catalyst was NaOH/Si-0.075, which maintains a high concentration of BAS (0.24 mmol g^{-1}) together with the addition of mesopores (0.21 mL g^{-1}). The results obtained in this work complete our understanding of synthesis–property–performance relationships of zeolite catalysts and open the way to rational fine-tuning of their properties.

Author contributions

Y. Z.: investigation (catalytic tests), formal analysis, and writing – original draft. A. G.: supervision, formal analysis, and writing – review & editing. J. R.: investigation (catalyst synthesis; XRD analysis; physisorption measurements). M. O.: conceptualization, supervision, and writing – review & editing. M. S.: conceptualization, funding acquisition, investigation (FTIR study), formal analysis, and writing – review & editing. All authors contributed to the final version of the manuscript.

Conflicts of interest

The authors declare that there is no competing interest.

Acknowledgements

M. O. and M. S. acknowledge the Czech Science Foundation for supporting this work through the project 20-12099S. The authors acknowledge Charles University Centre of Advanced Materials (CUCAM – OP VVV Excellent Research Teams, no. CZ.02.1.01/0.0/0.0/15_003/0000417) for providing infrastructure enabling this research and Plateau Technique du Pole Chimie Balard Montpellier for TEM measurements.

References

1 S. L. Suib, J. Přech, E. Szaniawska and J. Čejka, Recent Advances in Tetra-(Ti, Sn, Zr, Hf) and Pentavalent (Nb, V, Ta)

Metal-Substituted Molecular Sieve Catalysis, *Chem. Rev.*, 2022, **123**, 877–917.
2 Y. Li and J. Yu, Emerging applications of zeolites in catalysis, separation and host–guest assembly, *Nat. Rev. Mater.*, 2021, **6**, 1156–1174.
3 Z. Liu, Y. Wang and Z. Xie, Thoughts on the future development of zeolitic catalysts from an industrial point of view, *Chinese J. Catal.*, 2012, **33**, 22–38.
4 K. Möller and T. Bein, Mesoporosity–a new dimension for zeolites, *Chem. Soc. Rev.*, 2013, **42**, 3689–3707.
5 M. Hartmann, A. G. Machoke and W. Schwieger, Catalytic test reactions for the evaluation of hierarchical zeolites, *Chem. Soc. Rev.*, 2016, **45**, 3313–3330.
6 J. Pérez-Ramírez, C. H. Christensen, K. Egeblad, C. H. Christensen and J. C. Groen, Hierarchical zeolites: enhanced utilisation of microporous crystals in catalysis by advances in materials design, *Chem. Soc. Rev.*, 2008, **37**, 2530–2542.
7 R. Bai, Y. Song, Y. Li and J. Yu, Creating hierarchical pores in zeolite catalysts, *Trends Chem.*, 2019, **1**, 601–611.
8 A. H. Janssen, A. J. Koster and K. P. de Jong, Three-dimensional transmission electron microscopic observations of mesopores in dealuminated zeolite Y, *Angew. Chem., Int. Ed.*, 2001, **40**, 1102–1104.
9 D. Verboekend and J. Pérez-Ramírez, Design of hierarchical zeolite catalysts by desilication, *Catal. Sci. Tech.*, 2011, **1**, 879–890.
10 M. Shamzhy, M. Opanasenko, P. Concepción and A. Martínez, New trends in tailoring active sites in zeolite-based catalysts, *Chem. Soc. Rev.*, 2019, **48**, 1095–1149.
11 Z. Qin, L. Hafiz, Y. Shen, S. Van Daele, P. Boullay, V. Ruaux, S. Mintova, J.-P. Gilson and V. Valtchev, Defect-engineered zeolite porosity and accessibility, *J. Mater. Chem. A*, 2020, **8**, 3621–3631.
12 Z. Qin, Z. You, K. N. Bozhilov, S. K. Kolev, W. Yang, Y. Shen, X. Jin, J. P. Gilson, S. Mintova and G. N. Vayssilov, Dissolution Behavior and Varied Mesoporosity of Zeolites by NH_4F Etching, *Chem. Eur. J.*, 2022, **28**, e202104339.
13 X. Meng, F. Nawaz and F.-S. Xiao, Templating route for synthesizing mesoporous zeolites with improved catalytic properties, *Nano Today*, 2009, **4**, 292–301.
14 S. Abdulridha, J. Jiang, S. Xu, Z. Zhou, H. Liang, B. Mao, Y. Zhou, A. A. Garforth, Y. Jiao and X. Fan, Cellulose nanocrystals (CNCs) as hard templates for preparing mesoporous zeolite Y assemblies with high catalytic activity, *Green Chem.*, 2020, **22**, 5115–5122.
15 M. Choi, K. Na, J. Kim, Y. Sakamoto, O. Terasaki and R. Ryoo, Stable single-unit-cell nanosheets of zeolite MFI as active and long-lived catalysts, *Nature*, 2009, **461**, 246–249.
16 J. Zhao, Y. Yin, Y. Li, W. Chen and B. Liu, Synthesis and characterization of mesoporous zeolite Y by using block copolymers as templates, *Chem. Eng. J.*, 2016, **284**, 405–411.
17 Q. Sun, N. Wang, R. Bai, G. Chen, Z. Shi, Y. Zou and J. Yu, Mesoporogen-free synthesis of hierarchical SAPO-34 with low template consumption and excellent methanol-to-olefin conversion, *ChemSusChem*, 2018, **11**, 3812–3820.
18 H. Zhang, Y. Zhao, H. Zhang, P. Wang, Z. Shi, J. Mao, Y. Zhang and Y. Tang, Tailoring zeolite ZSM-5 crystal morphology/porosity through flexible utilization of Silicalite-1 seeds as templates: unusual crystallization pathways in a heterogeneous system, *Chem. Eur. J.*, 2016, **22**, 7141–7151.
19 K. Ding, A. Corma, J. A. Maciá-Agulló, J. G. Hu, S. Krämer, P. C. Stair and G. D. Stucky, Constructing hierarchical porous zeolites via kinetic regulation, *J. Am. Chem. Soc.*, 2015, **137**, 11238–11241.
20 Q. Zhang, A. Mayoral, O. Terasaki, Q. Zhang, B. Ma, C. Zhao, G. Yang and J. Yu, Amino acid-assisted construction of single-crystalline hierarchical nanozeolites via oriented-aggregation and intraparticle ripening, *J. Am. Chem. Soc.*, 2019, **141**, 3772–3776.
21 M. Alonso-Doncel, A. Peral, M. Shamzhy, J. Čejka, R. Sanz and D. Serrano, Fine-tuning hierarchical ZSM-5 zeolite by controlled aggregation of protozeolitic units functionalized with tertiary amine-containing organosilane, *Microporous Mesoporous Mater.*, 2020, **303**, 110189.
22 W. Cui, D. Zhu, J. Tan, N. Chen, D. Fan, J. Wang, J. Han, L. Wang, P. Tian and Z. Liu, Synthesis of mesoporous high-silica zeolite Y and their catalytic cracking performance, *Chinese J. Catal.*, 2022, **43**, 1945–1954.
23 H. S. Kamaluddin, X. Gong, P. Ma, K. Narasimharao, A. D. Chowdhury and M. Mokhtar, Influence of zeolite ZSM-5 synthesis protocols and physicochemical properties in the methanol-to-olefin process, *Mater. Today Chem.*, 2022, **26**, 101061.
24 F. Jiao, J. Li, X. Pan, J. Xiao, H. Li, H. Ma, M. Wei, Y. Pan, Z. Zhou and M. Li, Selective conversion of syngas to light olefins, *Science*, 2016, **351**, 1065–1068.
25 S. Gutiérrez-Rubio, M. Shamzhy, J. Čejka, D. P. Serrano, I. Moreno and J. M. Coronado, Vapor phase acylation of guaiacol with acetic acid over micro, nano and hierarchical MFI and BEA zeolites, *Appl. Catal., B*, 2021, **285**, 119826.
26 R. Barakov, N. Shcherban, P. Yaremov, I. Bezverkhyy, J. Čejka and M. Opanasenko, Hierarchical Beta zeolites as catalysts in a one-pot three-component cascade Prins–Friedel–Crafts reaction, *Green Chem.*, 2020, **22**, 6992–7002.
27 M. V. Opanasenko, M. V. Shamzhy, C. Jo, R. Ryoo and J. Čejka, Annulation of Phenols: Catalytic Behavior of Conventional and 2D Zeolites, *ChemCatChem*, 2014, **6**, 1919–1927.
28 K. Li, J. Valla and J. Garcia-Martinez, Realizing the commercial potential of hierarchical zeolites: new opportunities in catalytic cracking, *ChemCatChem*, 2014, **6**, 46–66.
29 D. Mehlhorn, J. Rodriguez, T. Cacciaguerra, A. Radu-Dorin, C. Cammarano, F. Guenneau, A. Gedeon, B. Coasne, M. Thommes, D. Minoux, C. Aquino, J.-P. Dath, F. Fajula and A. Galarneau, Revelation on the complex nature of mesoporous hierarchical FAU-Y zeolites, *Langmuir*, 2018, **34**, 11414–11423.
30 A. Galarneau, D. Mehlhorn, F. Guenneau, B. Coasne, F. Villemot, D. Minoux, C. Aquino and J.-P. Dath, Specific surface area determination for microporous/mesoporous

materials: the case of mesoporous FAU-Y zeolites, *Langmuir*, 2018, **34**, 14134–14142.

31 L. Desmurs, C. Cammarano, G. Ramona, R. Gaumard, T. Mineva, A. Sachse, J. D. Comparot, T. Cacciaguerra, D. Cot, O. Gimello, A. Galarneau and V. Hulea, Finding the compromise between Brønsted acidity and mesoporosity in hierarchical ZSM-5 zeolites, *ChemCatChem*, 2023, **15**, e202300167.

32 J. Meng, T. Cui, D. Bai, C. Li, X. Chen and C. Liang, Excellent catalytic performance over hierarchical ZSM-48 zeolite: cooperative effects of enhanced mesoporosity and highly-accessible acidity, *Fuel*, 2022, **324**, 124589.

33 K. A. Tarach, K. Góra-Marek, J. Martinez-Triguero and I. Melián-Cabrera, Acidity and accessibility studies of desilicated ZSM-5 zeolites in terms of their effectiveness as catalysts in acid-catalyzed cracking processes, *Catal. Sci. Tech.*, 2017, **7**, 858–873.

34 M. Shamzhy, M. Mazur, M. Opanasenko, W. J. Roth and J. Čejka, Swelling and pillaring of the layered precursor IPC-1P: tiny details determine everything, *Dalton Trans.*, 2014, **43**, 10548–10557.

35 J. W. M. Osterrieth, J. Rampersad, D. Madden, N. Rampal, L. Skoric, B. Connolly, M. D. Allendorf, V. Stavila, J. L. Snider, R. Ameloot, J. Marreiros, C. Ania, D. Azevedo, E. Vilarrasa-Garcia, B. F. Santos, X.-H. Bu, Z. Chang, H. Bunzen, N. R. Champness, S. L. Griffin, B. Chen, R.-B. Lin, B. Coasne, S. Cohen, J. C. Moreton, Y. J. Colón, L. Chen, R. Clowes, F.-X. Coudert, Y. Cui, B. Hou, D. M. D'Alessandro, P. W. Doheny, M. Dincă, C. Sun, C. Doonan, M. T. Huxley, J. D. Evans, P. Falcaro, R. Ricco, O. Farha, K. B. Idrees, T. Islamoglu, P. Feng, H. Yang, R. S. Forgan, D. Bara, S. Furukawa, E. Sanchez, J. Gascon, S. Telalović, S. K. Ghosh, S. Mukherjee, M. R. Hill, M. M. Sadiq, P. Horcajada, P. Salcedo-Abraira, K. Kaneko, R. Kukobat, J. Kenvin, S. Keskin, S. Kitagawa, K.-I. Otake, R. P. Lively, S. J. A. DeWitt, P. Llewellyn, B. V. Lotsch, S. T. Emmerling, A. M. Pütz, C. Martí-Gastaldo, N. M. Padial, J. García-Martínez, N. Linares, D. Maspoch, J. A. Suárez del Pino, P. Moghadam, R. Oktavian, R. E. Morris, P. S. Wheatley, J. Navarro, C. Petit, D. Danaci, M. J. Rosseinsky, A. P. Katsoulidis, M. Schröder, X. Han, S. Yang, C. Serre, G. Mouchaham, D. S. Sholl, R. Thyagarajan, D. Siderius, R. Q. Snurr, R. B. Goncalves, S. Telfer, S. J. Lee, V. P. Ting, J. L. Rowlandson, T. Uemura, T. Iiyuka, M. A. van der Veen, D. Rega, V. Van Speybroeck, S. M. J. Rogge, A. Lamaire, K. S. Walton, L. W. Bingel, S. Wuttke, J. Andreo, O. Yaghi, B. Zhang, C. T. Yavuz, T. S. Nguyen, F. Zamora, C. Montoro, H. Zhou, A. Kirchon and D. Fairen-Jimenez, How Reproducible are Surface Areas Calculated from the BET Equation?, *Adv. Mater.*, 2022, **34**, 2201502.

36 J. C. Broekhoff and J. H. Deboer, Studies on pore systems in catalysts XIII. Pore distributions from the desorption branch of a nitrogen sorption isotherm in the case of cylindrical pores B. Applications, *J. Catal.*, 1968, **10**, 377.

37 L. Desmurs, A. Galarneau, C. Cammarano, V. Hulea, C. Vaulot, H. Nouali, B. Lebeau, T. J. Daou, C. Vieira Soares, G. Maurin, M. Haranczyk, I. Batonneau-Gener and A. Sachse, Determination of Microporous and Mesoporous Surface Areas and Volumes of Mesoporous Zeolites by Corrected t-Plot Analysis, *ChemNanoMat*, 2022, **8**, e202200051.

38 V. Zholobenko, C. Freitas, M. Jendrlin, P. Bazin, A. Travert and F. Thibault-Starzyk, Probing the acid sites of zeolites with pyridine: quantitative AGIR measurements of the molar absorption coefficients, *J. Catal.*, 2020, **385**, 52–60.

39 O. V. Shvets, K. M. Konysheva, M. V. Shamzhy, M. V. Opanasenko, P. S. Yaremov, C. Xiao, X. Zou and J. Čejka, Mordenite nanorods and nanosheets prepared in presence of gemini type surfactants, *Catal. Today*, 2019, **324**, 115–122.

40 M. Shamzhy, B. Gil, M. Opanasenko, W. J. Roth and J. Čejka, MWW and MFI frameworks as model layered zeolites: structures, transformations, properties, and activity, *ACS Catal.*, 2021, **11**, 2366–2396.

41 A. Corma, V. Fornés, L. Forni, F. Márquez, J. Martinez-Triguero and D. Moscotti, 2,6-di-*tert*-butyl-pyridine as a probe molecule to measure external acidity of zeolites, *J. Catal.*, 1998, **179**, 451–458.

42 L. Lakiss, A. Vicente, J. P. Gilson, V. Valtchev, S. Mintova, A. Vimont, R. Bedard, S. Abdo and J. Bricker, Probing the Brønsted acidity of the external surface of Faujasite-type zeolites, *ChemPhysChem*, 2020, **21**, 1873–1881.

43 F. W. Jones, Estimation of Flame-Ionization Detector Relative Response Factors for Oligomers of Alkyl and Aryl Ether Polyethoxylates using the Effective Carbon Number Concept, *J. Chromatogr. Sci.*, 1998, **36**, 223–226.

44 J. S. Beck, J. C. Vartuli, W. J. Roth, M. E. Leonowicz, C. Kresge, K. Schmitt, C. Chu, D. H. Olson, E. Sheppard and S. McCullen, A new family of mesoporous molecular sieves prepared with liquid crystal templates, *J. Am. Chem. Soc.*, 1992, **114**, 10834–10843.

45 C. T. Kresge, M. E. Leonowicz, W. J. Roth, J. C. Vartuli and J. S. Beck, Ordered mesoporous molecular sieves synthesized by a liquid-crystal template mechanism, *Nature*, 1992, **359**, 710–712.

46 C. Baerlocher and L. B. McCusker, Database of Zeolite Structures: **https://www.iza-structure.org/databases/**.

47 T. Prasomsri, W. Jiao, S. Z. Weng and J. G. Martinez, Mesostructured zeolites: bridging the gap between zeolites and MCM-41, *Chem. Commun.*, 2015, **51**, 8900–8911.

48 G. Sartori, R. Ballini, F. Bigi, G. Bosica, R. Maggi and P. Righi, Protection (and deprotection) of functional groups in organic synthesis by heterogeneous catalysis, *Chem. Rev.*, 2004, **104**, 199–250.

49 H. S. Shin, M. Opanasenko, C. P. Cabello, R. Ryoo and J. Čejka, Surfactant-directed mesoporous zeolites with enhanced catalytic activity in tetrahydropyranylation of alcohols: Effect of framework type and morphology, *Appl. Catal., B*, 2017, **537**, 24–32.

50 M. Liu, O. Veselý, P. Eliášová, M. Shamzhy, P. Lyu and L. Grajciar, Identification of the most active sites for tetrahydropyranylation in zeolites: MFI as a test case, *Catal. Today*, 2020, **345**, 165–174.

51 M. V. Shamzhy, P. Eliašová, D. Vitvarová, M. V. Opanasenko, D. S. Firth and R. E. Morris, Post-Synthesis stabilization of

germanosilicate zeolites ITH, IWW, and UTL by substitution of Ge for Al, *Chem. Eur. J.*, 2016, **22**, 17377–17386.

52 M. V. Shamzhy, M. V. Opanasenko, F. S. D. O. Ramos, L. Brabec, M. Horáček, M. Navarro-Rojas, R. E. Morris, H. D. O. Pastore and J. Čejka, Post-synthesis incorporation of Al into germanosilicate ITH zeolites: the influence of treatment conditions on the acidic properties and catalytic behavior in tetrahydropyranylation, *Catal. Sci. Technol.*, 2015, **5**, 2973–2984.

53 M. M. Heravi, F. K. Behbahani, H. A. Oskooie and R. Hekmat Shoar, Mild and efficient tetrahydropyranylation of alcohols and dehydropyranylation of THP ethers catalyzed by ferric perchlorate, *Tetrahedron Lett.*, 2005, **46**, 2543–2545.

54 S. Molitorisová, Y. Zhang, M. Kubů, A. Li, Z. Tošner and M. Shamzhy, 2D-to-3D zeolite transformation for the preparation of Pd@MWW catalysts with tuneable acidity, *Catal. Today*, 2022, **390–391**, 109–116.

55 M. V. Shamzhy, O. V. Shvets, M. V. Opanasenko, L. Kurfiřtová, D. Kubička and J. Čejka, Extra-large-pore zeolites with UTL topology: control of the catalytic activity by variation in the nature of the active sites, *ChemCatChem*, 2013, **5**, 1891–1898.

56 M. Shamzhy and F. S. d O. Ramos, Tuning of acidic and catalytic properties of IWR zeolite by post-synthesis incorporation of three-valent elements, *Catal. Today*, 2015, **243**, 76–84.

57 G. Sartori and R. Maggi, Use of Solid Catalysts in Friedel–-Crafts Acylation Reactions, *Chem. Rev.*, 2006, **106**, 1077–1104.